Tie2 Receptor in Tumor-Infiltrating Macrophages Is Dispensable for Tumor Angiogenesis and Tumor Relapse after Chemotherapy

Moritz Jakab[1,2,3], Till Rostalski[1,2], Ki Hong Lee[1,2,3], Carolin Mogler[4], and Hellmut G. Augustin[1,2]

ABSTRACT

Tumor relapse after chemotherapy relies on the reconstruction of damaged tumor vasculature. In this context, proangiogenic Tie2-expressing macrophages have been suggested to serve as crucial instructors of tumor revascularization by secreting angiogenic factors while being closely associated with the vessel wall. Although the proangiogenic nature of $Tie2^+$ macrophages is well described, the functional contribution of macrophage Tie2 expression remains elusive. Here, we employed a Cre-loxP system to specifically delete *Tie2* in macrophages. In multiple syngeneic solid tumor models and two distinct chemotherapeutic treatment regimens, macrophage-expressed Tie2 did not contribute to primary tumor growth, tumor revascularization after chemotherapy, tumor recurrence, or metastasis. Exposing cultured murine macrophage cell lines and bone marrow–derived macrophages to hypoxia or stimulating them with Ang2 did not induce expression of Tie2 at the RNA or protein level. Furthermore, a comprehensive meta-analysis of publicly available single cell RNA sequencing datasets of human and murine tumor-infiltrating $CD11b^+$ myeloid cells did not reveal a transcriptionally distinct macrophage population marked by the expression of Tie2. Collectively, these data question the previously reported critical role of Tie2-expressing macrophages for tumor angiogenesis and tumor relapse after chemotherapy. Moreover, lack of Tie2 inducibility and absence of Tie2-positive macrophages in multiple recently published tumor studies refute a possible prognostic value of macrophage-expressed Tie2.

Significance: Multiple preclinical tumor models, cell stimulation experiments, and meta-analysis of published tumor single cell RNA sequencing data challenge the reported role of Tie2-positive macrophages for tumor angiogenesis, metastasis, and relapse after chemotherapy.

See related commentary by Zhang and Brekken, p. 1172

Introduction

Chemotherapy still represents the standard of care for most solid tumors. However, the efficacy of chemotherapeutic treatment remains relatively low for many tumors and a considerable fraction of responsive tumors will experience recurrence after extended treatment (1). The relapse mechanism depends on the existence of chemoresistant tumor cells that are kept in a hiatus by the harsh conditions of the tumor microenvironment. Paradoxically, chemotherapy exacerbates those conditions, which can in turn select for highly resistant clones and, thus, promote tumor recurrence (2).

One of the rate-limiting steps for tumors to resist chemotherapeutic insult and relapse subsequently is successful revascularization and restoration of perfusion. Tumor angiogenesis is driven by the hypoxic tumor microenvironment, which is caused by an abnormal tumor vasculature leading to vascular leakage and insufficient supply of oxygen. On the molecular level, hypoxia stabilizes hypoxia-inducible factor (HIF) in tumor cells (TC), which leads to the induction of angiogenic factors, such as vascular endothelial growth factor A (VEGFA; refs. 3, 4). Conversely, VEGFA secretion can directly promote sprouting angiogenesis, but presumably also lead to neovascularization by the recruitment of bone marrow-derived endothelial progenitor cells (EPC), a process referred to as vasculogenesis (5). EPC are believed to differentiate into mature endothelial cells (EC) and stabilize the vessel, while indirectly affecting angiogenesis by secreting EC-derived angiocrine factors (6, 7, 8). The nature and very existence of EPC continues to be highly controversial (9, 10, 11), as more evidence has been provided that the actual cell population contributing to tumor angiogenesis consists of bone marrow-derived macrophages (BMDM; refs. 12, 13, 14). These macrophages show high plasticity and can acquire EC-like properties *in vitro*, enabling them to form tubular structures similar to vessels (15). *In vivo*, BMDM were shown to express the EC marker genes vascular endothelial growth factor receptor 2 (*Vegfr2*) and TEK (*Tie2*), enabling them to home to gradients of VEGFA and angiopoietins, marking highly hypoxic areas in the tumor (16, 17). These Tie2-expressing macrophages (TEM) are mostly found in the perivascular space and accumulate in the tumor microenvironment after irradiation and chemotherapy, where they stimulate transient localized vascular permeability and promote tumor cell intravasation (18, 19). Systemic inhibition of Tie2 with rebastinib, a small molecule receptor tyrosine kinase (RTK) inhibitor, reduces tumor growth and metastasis, pointing towards a functional role of macrophage-expressed Tie2 (20, 21). TEMs were further shown to be

[1]European Center for Angioscience (ECAS), Medical Faculty Mannheim, Heidelberg University, Heidelberg, Germany. [2]Division of Vascular Oncology and Metastasis, German Cancer Research Center Heidelberg (DKFZ-ZMBH Alliance), Heidelberg, Germany. [3]Faculty of Biosciences, Heidelberg University, Heidelberg, Germany. [4]Institute of Pathology, TUM School of Medicine, Munich, Germany.

Note: Supplementary data for this article are available at Cancer Research Online (http://cancerres.aacrjournals.org/).

M. Jakab and T. Rostalski contributed equally in this article.

Corresponding Author: Hellmut G. Augustin, Department of Vascular Oncology, European Center for Angioscience (ECAS), Medical Faculty Mannheim, Heidelberg University, and Germany Cancer Research Center Heidelberg (DKFZ-ZMBH Alliance), Im Neuenheimer Feld 280, Heidelberg, D-69120, Germany. E-mail: augustin@angioscience.de

Cancer Res 2022;82:1353–64

doi: 10.1158/0008-5472.CAN-21-3181

stimulated by EC-derived angiopoietin 2 (Ang2), a ligand of Tie2, which fuels their inherent proangiogenic gene program. Interestingly, although TEMs home to gradients of Ang2, this migration is not dependent on the Ang/Tie-axis, but exerted through Ang2 and integrin interaction (22).

Recently, the genetic deletion of *Tie2* in macrophages was shown to exert dramatic effects on the tumor's ability to relapse after chemotherapy. Mechanistically, Tie2-dependent phosphorylation of RAC-alpha serine/threonine-protein kinase (AKT) prevented macrophages from apoptosis, whereas Tie2 expression alone was sufficient to promote vascular reconstruction (23). We have previously identified a tumor promoting macrophage population that is marked by C-C motif chemokine receptor 2 (CCR2)-expression (24). Yet, this macrophage population does not express Tie2. CCR2+ Tie2- macrophages are recruited to the primary tumor and the metastatic niche in an Ang2-dependent manner. Antibody-mediated blockade of Ang2 quenches the proinflammatory signature of EC, which leads to lower CCR2+ Tie2- macrophage infiltration and enhances chemotherapeutic treatment efficacy. Surprisingly, we did not to detect a distinct TEM population in this study in any of the employed models, questioning the functionality of macrophage-expressed Tie2 (24). These data are also in line with clinical findings showing that TEM infiltration does not correlate with ANG2 and VEGFA plasma levels, tumor stage, and anti-angiogenic treatment outcome in patients with colorectal cancer (25). To reconcile for the apparently discrepant findings of our previous work with the data reported by Chen and colleagues (23), this study was aimed at systematically investigating the functional role of Tie2 expression on macrophages during the revascularization of tumors after chemotherapy.

Materials and Methods

Mice

Tie2-KO mice were generated by breeding C57Bl/6 *LysM-Cre* mice (Jackson Laboratory, #004781) with $Tie2^{flox/flox}$ mice (26). C57BL/6 $Rosa26\text{-}YFP^{fl/fl}$ mice were crossed with C57Bl/6 *LysM-Cre* to constitutively label myeloid cells. For all experiments, 8- to 12-week-old mice of both genders were used if not otherwise indicated. Mice were housed in sterile cages, maintained in a temperature-controlled room and fed autoclaved water and food *ad libitum*. All animals were monitored daily for signs of disease. Ear punches were used for genotyping and tail tips were collected for re-genotyping after experiments. Mice were euthanized by cervical dislocation. All experiments were performed according to the guidelines of the institutional and governmental Animal Care and Use Committees and approved by the Regierungspräsidium Karlsruhe (permits G287/16, DKFZ305, DKFZ370).

Tumor implantation

MCA205, B16F10, Lewis lung carcinoma (LLC), and E0771 tumor cells (5×10^5 each) in 200 μL PBS were injected subcutaneously into the left ventral flank of 6 to 8 weeks old Tie2-KO and Ctrl littermates. All mice were routinely checked for humane endpoint criteria. Tumor volumes were determined by caliper measurements (tumor volume = 0.5 × length × width × width).

Chemotherapy

For chemotherapeutic intervention experiments, mice were treated with either doxorubicin (2.5 mg/kg in DMSO, intratumorally) or cyclophosphamide (65 or 130 mg/kg in PBS, intraperitoneally) either at the indicated time points after tumor implantation or when the primary tumor had reached a volume of approximately 150 mm^3. Mice in the control group were treated with the same volume of PBS at the identical time points.

Resection experiments

LLC tumors were implanted as described above and primary tumors were grown for 12 days. The mice then received a high dose (130 mg/kg) of cyclophosphamide and tumors were surgically removed 19 days after inoculation. After surgery, mice were routinely checked for the experimental endpoint criteria. All mice were killed at the same time point and the metastatic burden was assessed.

Zymosan A–induced peritonitis model

To induce acute peritonitis, Tie2-KO or Ctrl mice were injected intraperitoneally with 10 μg of Zymosan A (from saccharomyces cerevisiae; Sigma) per mouse or PBS vehicle control. After 24 hours, mice were killed by cervical dislocation and a small incision was made to expose the peritoneum without damage. The peritoneal cavity was washed with 10 mL ice cold PBS and the lavage was carefully collected by avoiding any bleeding. The lavage volume was recorded and peritoneal lavage samples were subjected to flow cytometric analysis.

Immunofluorescence staining

Fresh tissue samples were embedded in Tissue-TEK OCT and cut into 7-μm-thick sections for IF staining. Cryosections were fixed and permeabilized in ice-cold methanol for 10 minutes at −20°C. Following washings, sections were blocked in 10% ready-to-use normal goat serum or 10% donkey serum for 1 hour at room temperature, followed by overnight incubation with rat anti-CD31 (BD Biosciences) diluted in blocking buffer at 4°C. Slides were stained for 1 hour with anti-rat Alexa Fluor 568 antibody at room temperature. Cell nuclei were counterstained with 1:2,000 Hoechst 33342 (Sigma) and sections were mounted with DAKO mounting medium. After each staining step, samples were washed three times in TBS-T for 5 minutes.

Image acquisition and vessel area quantification

Images were taken as whole area tile scans using an Axio Scan.Z1 slide scanner, and image analysis was performed in Fiji using automated thresholding techniques. The CD31-positive vessel area was then normalized to the total tissue area.

Cell culture

Cells used in the present study were maintained at 37°C, high humidity and 5% CO_2. All cell lines (MCA205, B16F10, EO771, LLC, J774, RAW 264.7, isolated bone marrow-derived myeloid cells) were cultured in DMEM high glucose (Gibco) supplemented with 10% (v/v) FCS and 100 U/mL penicillin/streptomycin (Sigma). Cell identity was confirmed by morphology and cultured cells were checked regularly for mycoplasma contamination by PCR and subcultured upon reaching 80% to 90% confluency. For this, cells were either detached by scraping (J774, RAW 264.7) or by treatment with trypsin-EDTA (MCA205, B16F10, EO771, LLC).

In vitro stimulation

For stimulation assays, isolated bone marrow-derived myeloid cells, J774 and RAW267 cells were seeded into 6-well plates. At around 80% confluency, cells were washed with PBS and stimulated for 24 hours with 400 μmol/L cobalt-(II)-hexahydrate (Sigma) and/or 400 ng/ml recombinant mouse Ang2 (RnD Systems). For directly mimicking low oxygen conditions, cells were cultured in a 1% oxygen cell culture chamber for 24 hours. Cells were then processed for further analysis under hypoxic conditions.

Isolation of bone marrow–derived macrophages

Bone marrow–derived macrophages were isolated from the bones of the lower extremities and the pelvis of 6- to 8-week-old mice. For this purpose, bones were crushed on ice using a mortar. The bone marrow was filtered and the resulting single cell suspension was plated under sterile conditions in 50 mL of DMEM medium supplemented with 10% FCS, 100 U/mL penicillin, 100 μg/mL streptomycin. After overnight incubation, the nonadherent supernatant, containing the myeloid progenitor cells, was harvested and seeded into 6-well plates at a concentration of 1.9×10^5 cells/cm^2. The cells were then stimulated for 7 days with 20 ng/mL recombinant M-CSF (Peprotech) in supplemented DMEM to generate a differentiated macrophage culture.

Flow cytometry

To reduce nonspecific binding to cells bearing Fc receptors, preincubation of cells with anti-mouse CD16/CD32 (eBioscience) was performed prior to all antibody stainings. Dead cells were excluded by FxCycle Violet (Thermo Fisher Scientific) staining. Stained cells were analyzed using a BD FACSCanto II or analyzed and FACS-sorted using a BD Aria cell sorting platform. The frequencies of individual cell populations were quantified with FlowJo software. FACS antibodies used in this study were: rat anti-CD11b (eBioscience, PE-Cy7), rat anti-CD31 (BioLegend, FITC), rat anti-F4/80 (BioLegend, PE), rat anti-Ly6C (BioLegend, APC-Cy7), rat anti-Ly6G (BioLegend, Pacific Blue), rat anti-Tie2 (Invitrogen, APC) and rat anti-CD206 (BD Biosciences, Alexa Fluor 488). Single-stained controls and an unstained control were used for compensation, rat-IgG1 κ (eBioscience, APC) was used as isotype control.

Cell isolation

TIMs

Primary tumors were removed and minced using scissors. Minced tissue pieces were digested with Liberase digestion enzyme mix at 37°C for 20 minutes. Single cell suspensions were prepared by passing digested tissues through 19G cannula syringes and filtering through a 100 μmol/L cell strainer. Liberase digestion was stopped by adding FCS. Red blood cells were lysed with 1× ACK (ammonium chloride potassium) lysis buffer. For cell sorting, single cell suspensions were incubated with CD11b microbeads (Miltenyi) according to the manufacturer's instructions and CD11b$^+$ cells were enriched using LS columns (Miltenyi). The enriched cell population was then further processed for flow cytometric analyses as described above.

Blood and peritoneal lavage

Peritoneal lavage and blood samples were spun down and the resulting cell pellets were resuspended in 1× ACK lysis buffer. After red blood cell lysis, single cell suspensions were stained and analyzed by flow cytometry as described above.

IHC

Zinc-fixed murine tissue samples were paraffin embedded and cut into 7 μm sections. Sections were dewaxed and rehydrated. All images were acquired as whole-area tile scans using an Axio Scan.Z1 slide scanner (Zeiss).

CD31$^+$ vessel area analysis

IHC stainings against CD31 (Dianova; SZ31) were performed automatically (Leica Bond Max) according to standard protocols (pretreatment EDTA buffer pH9 for 30 minutes) and visualized using the Bond Polymer Refine Detection Kit.

Necrosis analysis

Sections were stained with hematoxylin and eosin and analyzed in a blinded manner by a board-certified pathologist (C. Mogler, TUM, Munich, Germany) to assess the percentage of the necrotic area per tumor.

RT-qPCR

RNA isolation

Total RNA of FACS-sorted mouse cells was isolated using the Arcturus PicoPure RNA Isolation Kit (Thermo Fisher Scientific) according to the manufacturer's instructions. Total RNA of cultured cells was isolated using the GenElute Mammalian Total RNA Purification Kit (Merck) according to the manufacturer's instructions. Total RNA from tissues was isolated by smashing tissue pieces in TRIzol (Thermo Fisher Scientific), followed by chloroform extraction. Isolated RNA was then purified using the RNeasy Mini Kit (Qiagen) according to the manufacturer's instructions.

Reverse transcription of RNA

Total RNA was reverse transcribed by using the QuantiTect Reverse Transcription Kit (Qiagen) according to the manufacturer's instructions.

RT-qPCR

Gene expression analysis was performed by qPCR using TaqMan reactions and the Lightcycler 480 (Roche) or the StepOnePlus Real-Time PCR system (Applied Biosystems). The following TaqMan probes (Thermo Fisher Scientific) were used: *Actb*-Mm00607939_s1 and *Tek*-Mm00443254_m1. Gene expression levels were assessed by comparing the C_t values of each sample with a standard curve and normalizing it to the expression of β-actin (Actb). Gene expression is displayed as: $\frac{1}{\Delta C_t}$.

Western blot analysis

Protein extracts from cell cultured cells were analyzed by Western blot analysis as described previously (Inverso and colleagues 2021). The following primary antibodies were used: anti-mouse Hif1α (Novus Biologicals), anti-mouse α/β-tubulin (Cell Signaling Technology). Anti-rabbit:HRP (Invitrogen) was used as secondary antibody and detected by SuperSignal West Pico PLUS Chemiluminescent Substrate (Thermo Fisher Scientific). Images were acquired with Amersham Imager 600 (GE Healthcare).

Single cell RNA sequencing (scRNA-seq) meta-analysis

scRNA-seq data integration

Filtered and normalized human and mouse count matrices were downloaded from the following accession codes: GSE146409 (27), GSE127465 (28), GSE154763 (29), GSE114727 (30), GSE121861 (31), GSE125588 (32), GSE119352 (33), GSE163120 (34), GSE136001 (35), and E-MTAB-7427 (36). Human and mouse datasets were integrated using Seurat version 4 (37). In brief, Seurat objects were constructed for each individual human and mouse dataset using the CreateSeuratObject function with default parameters. Information regarding the cancer entity was stored in the metadata. Both, human and mouse Seurat objects were then integrated using the reciprocal PCA (rPCA) workflow with default parameters. Subsequently, the integrated count matrices were scaled, principal component analysis (PCA) performed and UMAP visualization was carried out on the top 50 principal components for the integrated datasets.

scRNA-seq data visualization

Tie2-expressing myeloid cells were identified as cells with *TEK* or *Tek* expression >0. The expression level was not considered.

Figure 5C, **E**, and **F**: Percentage of cells with *TEK* or *Tek* expression >0 within the integrated dataset was calculated and visualized in a pie chart.

Figure 5D + Supplementary Fig. S4C: Tie2+ myeloid cells were visualized by selecting cells with *TEK/Tek* expression >0, using the WhichCells function in Seurat. The defined subset was then highlighted using the cells.highlight parameter of the DimPlot function in Seurat.

Supplementary Figs. S4C and S4D: Nonintegrated Tie2+ myeloid cells containing datasets were subsetted. Count matrices were scaled and PCA was performed. UMAP and shared nearest-neighbors graph construction was carried out on the top 15 principal components, while clusters were identified with the resolution parameter set to 0.3.

Supplementary Figs. S4E and S4F: Tie2+ myeloid cells were subsetted from the integrated datasets. Clustering analysis was performed as described above. The normalized expression of each gene within the vascular gene panel and for each Tie2+ myeloid cell was summed and stored in the metadata of the Seurat object. The vascular gene expression was then visualized on the UMAP or correlated with *TEK* or *Tek* expression using the FeatureScatter function in Seurat.

Results

TEMs do not affect tumor relapse after chemotherapy

To study the functional contribution of macrophage-expressed Tie2 during the process of tumor re-vascularization after chemotherapeutic treatment, we generated a mouse model with conditional myeloid cell-specific *Tie2* gene knockout. For this purpose, *Tie2* floxed mice were crossed to the *LysM-Cre* deleter line to generate transgenic animals with a specific homozygous *Tie2* deletion in the myeloid lineage (*LysM-Cre* × $Tie2^{fl/fl}$). The specificity of the constitutive driver was validated by crossing *LysM-Cre* mice to *YFP* reporter mice, fluorescently labeling all cell populations with recombination. Consistent with earlier reports (38), we did not detect recombination in vascular cells, but observed that approximately 75% of blood-circulating $CD11b^{+}$ myeloid cells were marked by YFP expression (Supplementary Fig. S1A).

TEMs have recently been reported to promote tumor relapse after chemotherapy (23). In this study, a transgenic mouse line was used in which the animals with myeloid-specific gene deletion of *Tie2* were also heterozygous knockout for *Tie2* in all other cells, whereas control animals were homozygous *Tie2* wild-type mice. To avoid any confounding gene dosage effects in the vascular cell compartment, we reproduced the reported experiment of this study employing *LysM-Cre* × $Tie2^{fl/fl}$ transgenic mice by injecting MCA205 fibrosarcoma cells subcutaneously in Cre+ $Tie2^{fl/fl}$ (Tie2-KO) and Cre− $Tie2^{fl/fl}$ littermate control (Ctrl) mice (**Fig. 1A**). The animals were treated with a single dose of either doxorubicin (DOX; intratumorally) or cyclophosphamide (CTX; systemic) or PBS (CON) after 12 days of tumor growth. Therapy response and subsequent tumor relapse were comparatively analyzed (**Fig. 1B**). PCR amplification of the *Tie2* gene locus in isolated TIMs confirmed the genetic deletion of *Tie2* in the macrophage lineage in Tie2-KO animals (Supplementary Fig. S1B).

As expected, single shot chemotherapy led to a significant transient growth delay compared to the PBS control group (Supplementary Fig. S1C). However, in contrast to the previous report, we did not observe a difference in tumor progression and tumor relapse between Tie2-KO and Ctrl mice after chemotherapeutic intervention. Although we did observe complete remission in some mice, these observations did not depend on the genotype, but were rather linked to differences in the size of the primary tumor at the time point of chemotherapeutic intervention (**Fig. 1B**). Correspondingly, we also did not detect differences in the CD31-positive vessel area and the extent of intratumoral necrosis between Tie2-KO and Ctrl mice (**Fig. 1C** and **D**). Moreover, chemotherapy treated mice were able to fully reconstruct their vascular system, as the treatment groups and the PBS control group did not display differences in vessel area or necrosis at the experimental end point either.

To further validate these findings, we adopted three widely used and well described murine tumor models, namely the LLC model, the B16F10 melanoma model and the E0771 breast cancer model. Subcutaneous implantation of these tumor cell lines into Tie2-KO and WT mice was followed by single shot chemotherapy either local DOX or systemic CTX and therapy response and tumor relapse were monitored thereafter. As we had observed a tumor size-dependent remission in the MCA205 tumor model following chemotherapy, we size matched tumors in the B16F10 and E0771 models, rather than treating the mice at the same time point. Confirming and extending our previous results, myeloid-specific deletion of Tie2 had no effect on primary tumor relapse in any of the tumor models (**Fig. 1E** and **F**) and similarly did not affect tumor necrosis and revascularization (Supplementary Figs. S1D and S1E). These findings are in stark contrast to the previous study reporting a strong effect of TEMs on tumor relapse after chemotherapy (23). Instead, we conclude that the genetic strategy of this study was flawed and did not allow to specifically and selectively study the effect of Tie2 expressed by macrophages on tumor growth. Employing four different tumor models, the present study establishes that TEMs do not promote tumor vascularization and regrowth after chemotherapy.

Tie2 expression on macrophages is not related to or induced by increasing chemotherapeutic dosage

TIMs have been reported to upregulate Tie2 in response to hypoxia and proinflammatory signals, such as Ang2 (23, 39). We therefore hypothesized that higher concentrations of the cytotoxic agents may result in more severe vascular disruption. This, in turn, may generate a more hypoxic and inflamed microenvironment, which may result in a stronger induction of Tie2 expression in macrophages. To test this hypothesis, we implanted LLC tumors subcutaneously, which were previously shown to be infiltrated by TEMs upon chemotherapy (40), in Tie2-KO and Ctrl animals and treated the mice at three consecutive time points with a single dose (medium dose) or two doses (high dose) of cyclophosphamide (**Fig. 2A**). As expected, higher concentrations of CTX resulted in an extended delay of tumor regrowth and a more disrupted vascular network, as in contrast to our initial experiments, tumors of the medium and high dose treated groups were diminished in their ability to reconstruct their vascular system. This was evidenced by a significantly decreased CD31 tumor vessel area compared with the PBS control at the experimental end point (**Fig. 2B** and **C**). However, we did not observe differences between the Tie2-KO and Ctrl group in their ability to re-establish the tumor vascular system and consequently did not identify reduced tumor recurrence in the Tie2-KO group for the medium and the high-dose treatment regimen (**Fig. 2A**; Supplementary Fig. S2A).

As we did not observe phenotypic differences at the experimental endpoint, we characterized the TIMs for both genotypes immediately after chemotherapeutic insult. To this end, we isolated TIMs 1 and 2 days after the last CTX injection in the medium dose model and determined Tie2 expression at the protein and RNA level using flow

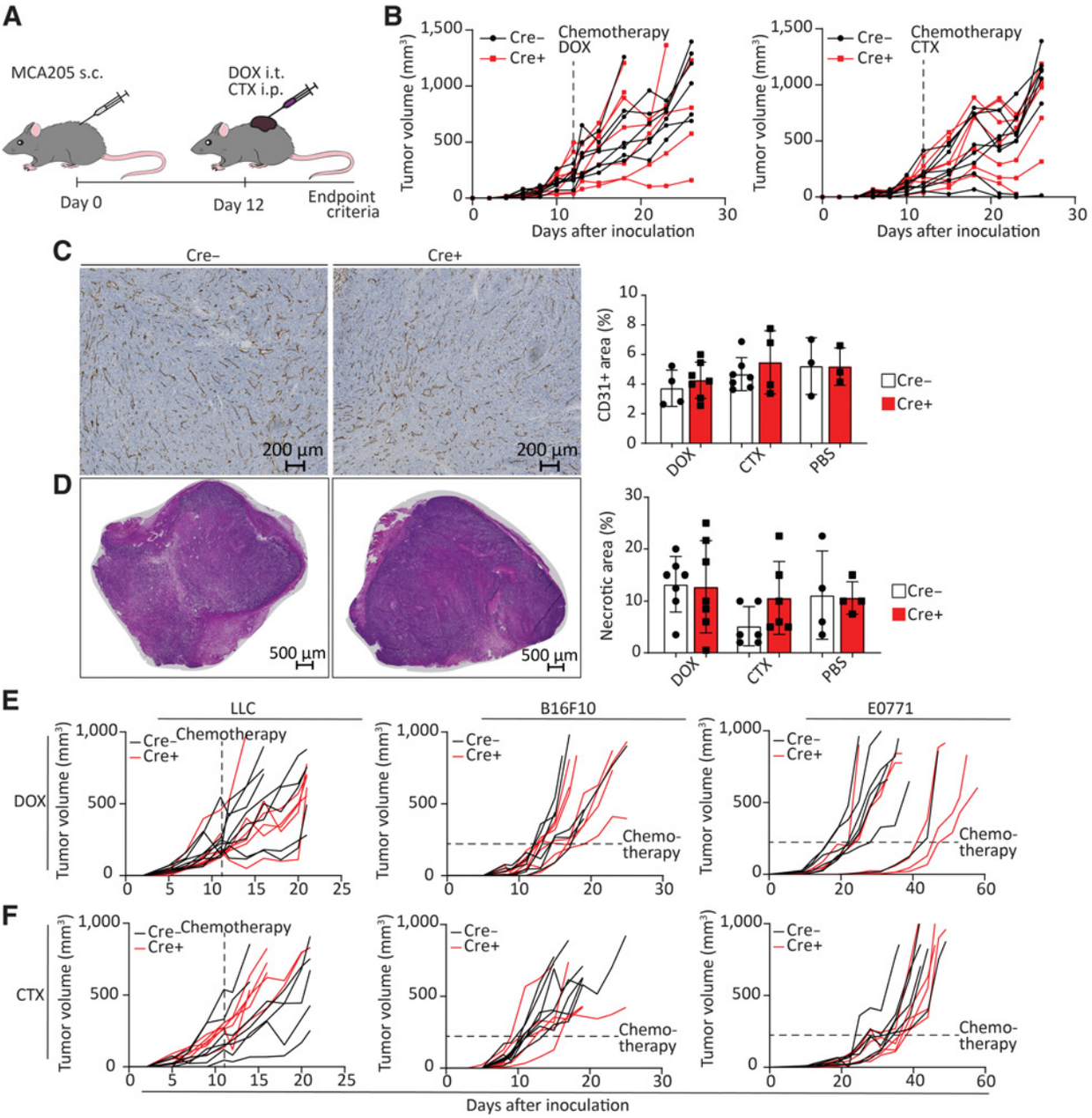

Figure 1.

A, Schematic overview of the experimental approach. **B,** MCA205 primary tumor growth curves of individual mice; the dashed lines indicate the time point of chemotherapeutic intervention with DOX (left) or CTX (right). **C,** Representative immunohistochemistry images of CD31 staining of tumor sections from Ctrl (left) and Tie2-KO (middle) mice after treatment with DOX at the experimental endpoint, with quantification of the respective $CD31^+$ area for each treatment group (right). Scale bars, 200 µm. **D,** Representative hematoxylin and eosin staining of tumor sections of Ctrl (left) and Tie2-KO (middle) mice after treatment with DOX at the experimental endpoint, with quantification of the necrotic area for each treatment group (right). Scale bars, 500 µm. **E** and **F,** Primary tumor growth curves of individual mice for LLC (left), B16F10 (middle), and E0771 (right) cell lines. The dashed lines indicate the time point of chemotherapeutic intervention with DOX (**E**) or with CTX (**F**). Data are shown as mean ± SD. The statistical analysis was performed using Student *t* test; $n = 3$–7 (**A–D**) and $n = 4$–8 (**E**).

cytometry with a validated anti-Tie2 antibody (Supplementary Figs. S2B and S2C) and RT-qPCR. Surprisingly, mean Tie2 fluorescence intensity (MFI) did not differ between Tie2-KO and Ctrl mice at day 1 and day 2, indicating a general lack of Tie2 protein expression in TIMs (**Fig. 2D**). Moreover, while we observed a small subset of Tie2+ macrophages in the flow cytometric analysis, we detected a similarly sized population in the Tie2-KO group, as well as in the isotype control antibody-stained samples (**Fig. 2E**). Comparing the frequency of Tie2+ macrophages for each Tie2-stained sample to its respective isotype antibody-stained control revealed no differences indicative of

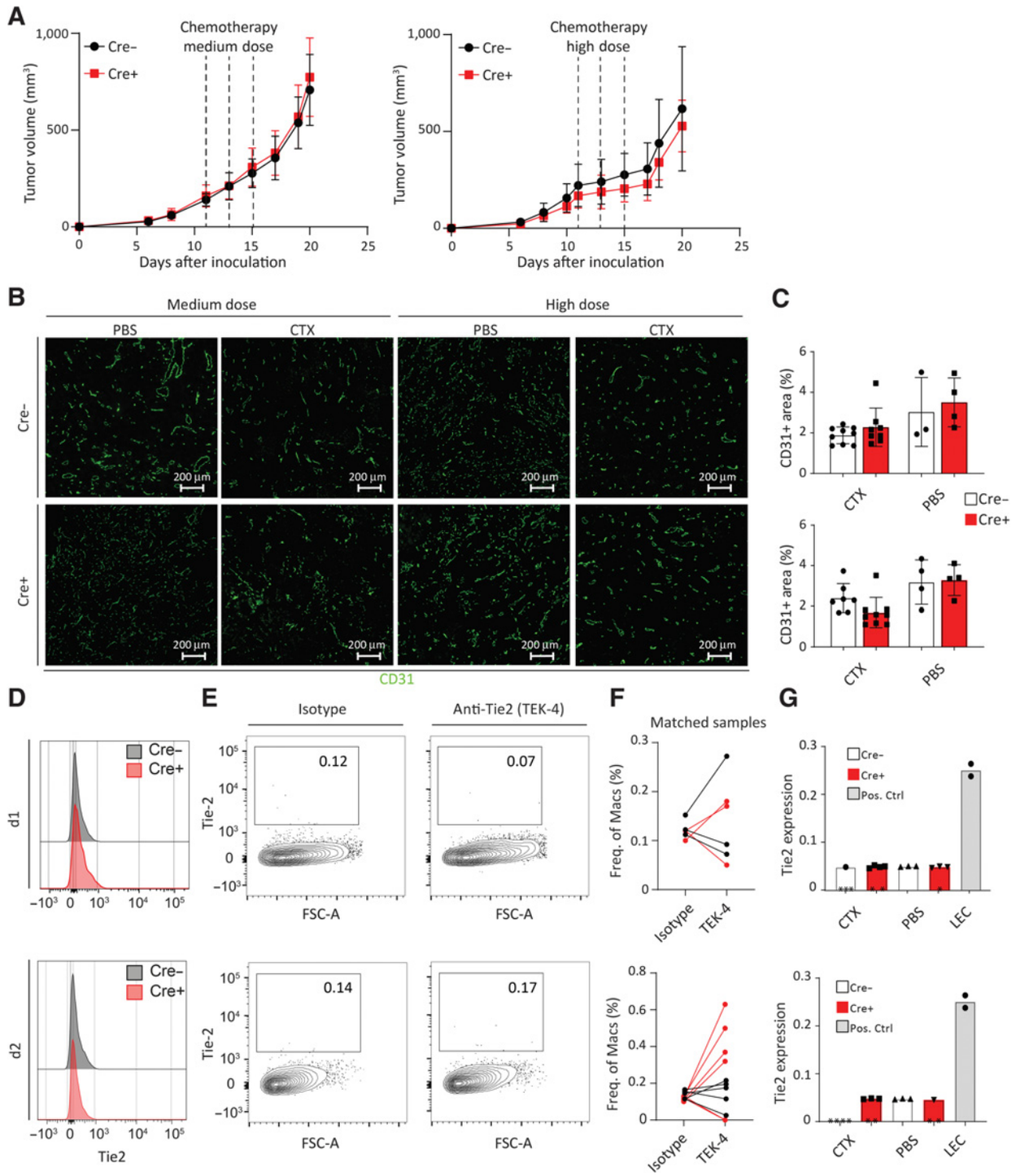

Figure 2.

A, LLC primary tumor growth curves for Ctrl and Tie2-KO mice, treated with medium dose (left) or high dose (right) CTX. The dashed lines indicate the time point of chemotherapeutic intervention; $n = 7–9$. **B,** Representative immunofluorescence images of CD31 staining on tumor sections of Ctrl (top) and Tie2-KO (bottom) mice after treatment with medium dose (left) or high dose (right) CTX and PBS controls at the experimental endpoint. Scale bars, 200 µm. **C,** Quantification of respective $CD31^+$ area of tumor sections for medium dose (top) and high dose (bottom) treatment compared with PBS controls. **D,** Representative histograms of Tie2 staining intensity of TIMs in Ctrl and Tie2-KO mice 1 day (top) or 2 days (bottom) after medium dose treatment. **E,** Representative contour plots of isotype control-stained (left) or Tie2-stained (right) TIMs in Ctrl mice 1 day (top) or 2 days (bottom) after medium dose treatment. **F,** Pairwise analysis of Tie2+ macrophage frequencies of the total TIM pool between matched isotype control–labeled and Tie2-stained samples in Ctrl mice (black) and Tie2-KO (red) 1 day (top) or 2 days (bottom) after medium dose treatment. **G,** Relative *Tie2* mRNA expression in TIMs in Ctrl and Tie2-KO mice 1 day (top) or 2 days (bottom) after treatment with medium dose CTX or PBS. Data are shown as mean ± SD. The statistical analysis was performed using Student *t* test, $n = 3–9$.

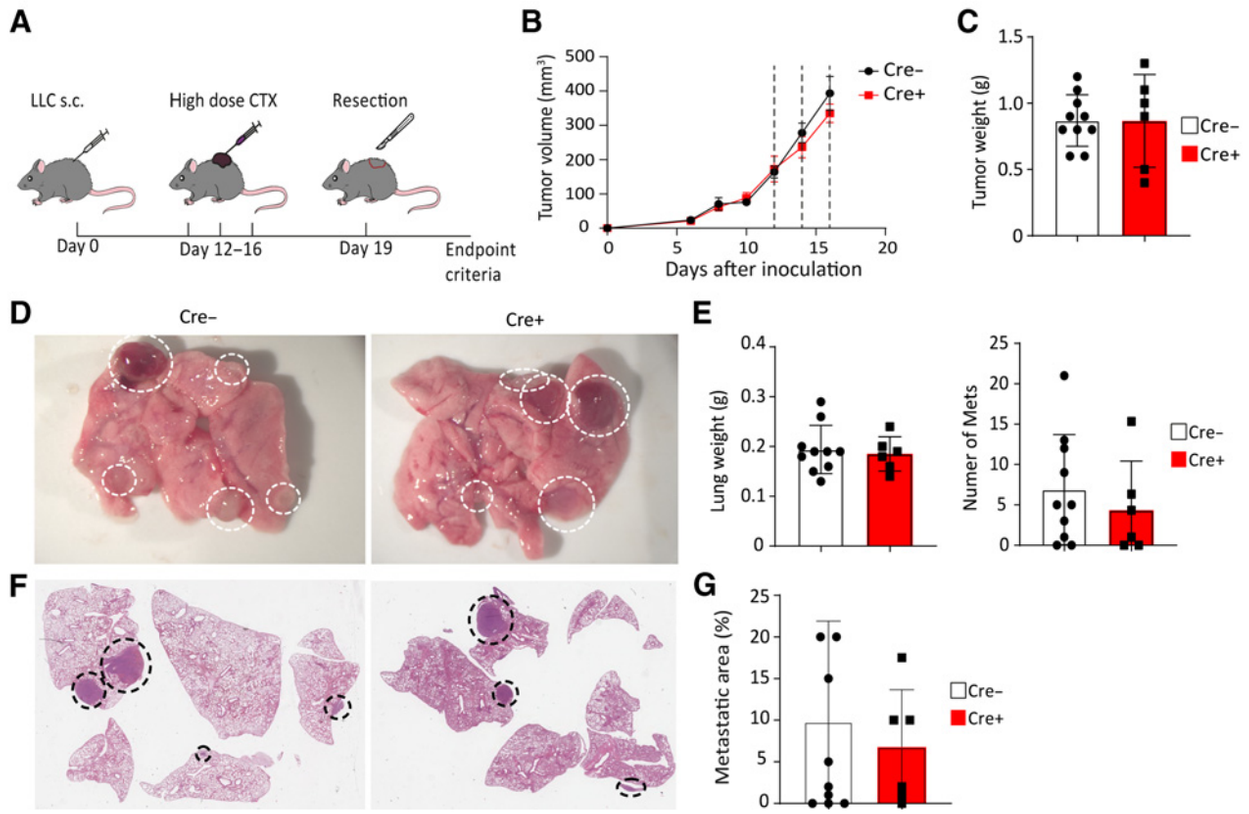

Figure 3.

A, Schematic overview of tumor resection model. **B,** Growth curves of LLC primary tumor until the time point of resection; dashed lines indicate the time points of chemotherapeutic intervention, $n = 6–10$. **C,** Primary tumor weights at the time point of resection. **D,** Representative images of metastatic lungs in Ctrl (left) and Tie2-KO (right) mice. White circles, macroscopic metastases. **E,** Lung weights (left) and number of metastatic foci (right) in Ctrl and Tie2-KO mice at the experimental endpoint. **F,** Representative hematoxylin and eosin staining of sectioned metastatic lungs of Ctrl (left) and Tie2-KO (right) mice. Black circles, areas with metastatic nodules. **G,** Quantification of the metastatic area of respective lung sections. Data are shown as mean ± SD. The statistical analysis was performed using Student *t* test, $n = 6–10$.

nonspecifically stained subsets (**Fig. 2F**). These results were further substantiated by assessing *Tie2* expression at the transcriptional level, because we did not identify significant differences between the PBS- and CTX-treated groups, nor between Tie2-KO and Ctrl mice (**Fig. 2G**). Moreover, *Tie2* expression was barely detectable at the mRNA level, with roughly half of the samples displaying Ct-values below the detection limit in the RT-qPCR analysis. These observations put the biological relevance of macrophage expressed Tie2 in question, as, in strong contrast to previously published work, we did not find a contribution of macrophage-expressed Tie2 during tumor relapse after chemotherapy and, more importantly, could not detect robust expression of the Tie2 receptor in macrophages.

Macrophage-expressed Tie2 is not involved in the metastatic spread of cancer cells

At the molecular level, TEMs have been shown to secrete pro-angiogenic factors, such as VEGFA, which promotes tumor angiogenesis, but also leads to transient vascular permeability and thereby enables tumor cells to intravasate and metastasize (18). Systemic blockade of Tie2 with the small molecule inhibitor rebastinib successfully inhibited this process and led to a reduced metastatic burden (20). As we were not able to establish biologically relevant functional readouts of macrophage-expressed Tie2 during tumor revascularization and tumor angiogenesis, we hypothesized that rebastinib may probably act on non-macrophage cell populations of the tumor microenvironment. To test this, we applied an experimental metastatic resection model combined with neoadjuvant chemotherapy to amplify the Tie2-inducing stimulus. LLC tumors were towards this end subcutaneously implanted in Tie2-KO and Ctrl mice and treated with high dose CTX 12-, 14-, and 16-days post-implantation. Subsequently, primary tumors were surgically removed after 19 days of tumor growth and the post-surgical development of lung metastases was monitored (**Fig. 3A**). In line with our previous findings, primary tumor growth and primary tumor weight did not differ at the time of resection between the different experimental groups (**Fig. 3B** and **C**). Likewise, macroscopic analysis of the metastatic lungs revealed no differences in metastatic burden as evidenced by the number of ectopic macro-metastatic nodules and the total lung weight (**Fig. 3D** and **E**). Metastatic lungs were sectioned for histologic analysis and the metastatic area was quantitated. Again, we did not observe a difference between Tie2-KO and Ctrl mice (**Fig. 3F** and **G**), arguing against a contribution of macrophage-derived Tie2 during metastatic dissemination.

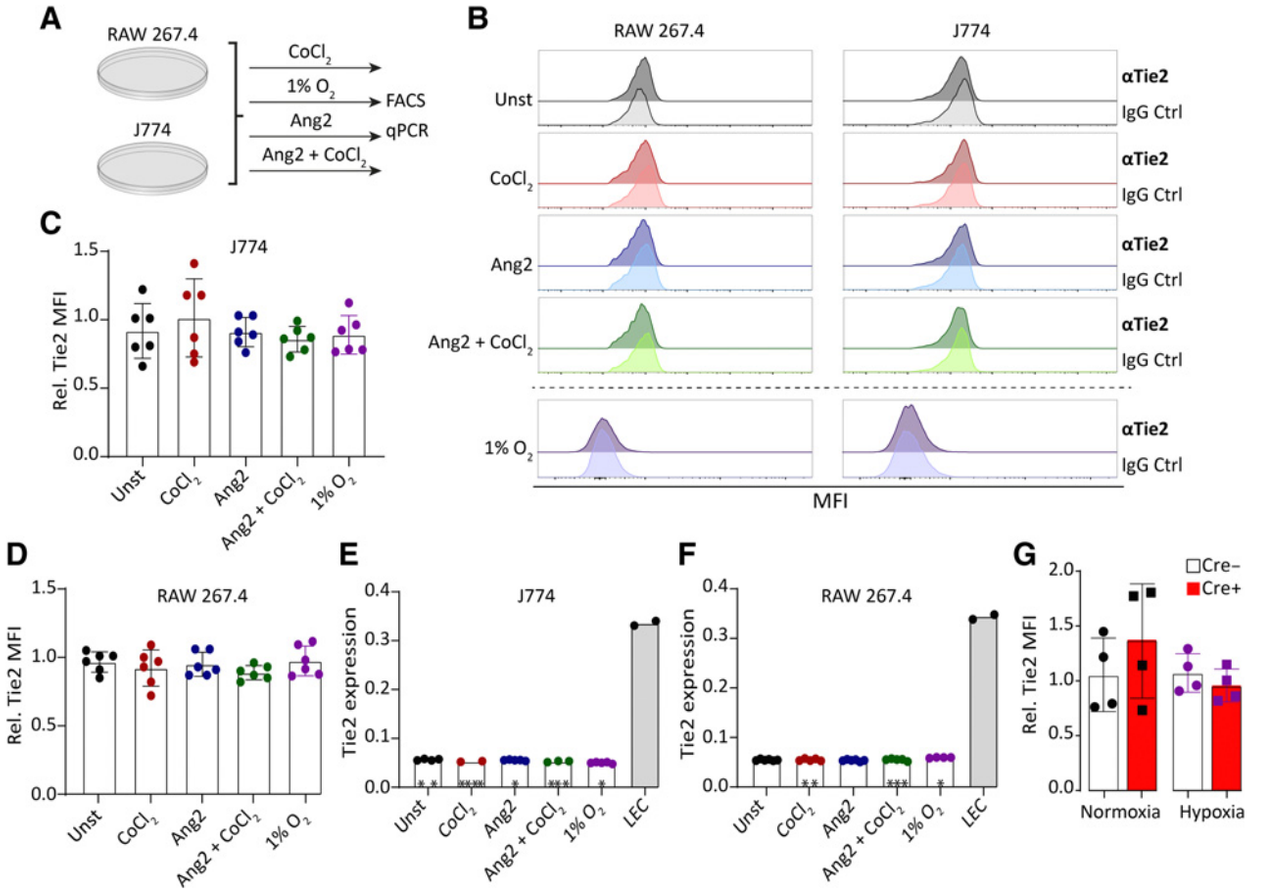

Figure 4.

A, Schematic overview of the *in vitro* approach. **B,** Representative histograms of Tie2-stained (dark line, top) or corresponding isotype control-stained (light line, bottom) of RAW267.4 (left) and J774 (right) cells after 24 hours of culture under stimulating or control conditions. **C** and **D,** Quantification of the relative Tie2-MFI (fold change over isotype control) after culture for 24 hours in stimulating or control conditions of J774 (**C**) and RAW267.4 (**D**) cells. **E** and **F,** Corresponding relative *Tie2* mRNA expression after 24 hours under stimulating or control conditions in J774 cells (**E**) as well as in RAW267.4 cells (**F**). Stars indicate samples with C_t values for Tie2 below the detection limit. **G,** Relative Tie2-MFI of bone marrow–derived myeloid cells isolated from Ctrl or Tie2-KO animals after 24 hours of culture under normoxic (left) and hypoxic (right) conditions. Data are shown as mean ± SD. The statistical analysis was performed using one-way ANOVA with Bonferroni posttest, $n = 6$ (**C–F**) or Student t test, $n = 4$ (**G**).

Cultured macrophage cell lines and primary myeloid cells do not upregulate Tie2 upon hypoxic challenge or Ang2 stimulation

Multiple lines of experimentation in preclinical tumor models did not support a functional role of macrophage-expressed Tie2 during tumor growth. Moreover, Tie2 expression in TIMs was not induced upon chemotherapy. To validate the ability of macrophages to express Tie2, we employed two widely used murine macrophage-like cell lines, RAW267.4 and J774, with the aim to induce Tie2 expression. Previous studies have shown that both exposure to hypoxia and stimulation with Ang2 may induce expression of Tie2 in macrophages (23, 39). We therefore exposed the cell cultured cells to either hypoxia (1% O_2), the maximum tolerable dose of $CoCl_2$, a chemical stabilizer of HIF (Supplementary Fig. S3A), recombinant Ang2, or a combination of $CoCl_2$ and Ang2. Following stimulation, the expression of Tie2 was quantified at the protein and mRNA level by means of flow cytometry and RT-qPCR (**Fig. 4A**). In line with the tumor experiments, stimulation of cultured macrophage cell lines did not induce Tie2 at the protein level, as demonstrated by identical Tie2-MFI in the antibody-stained samples and their respective isotype controls (**Fig. 4B**). Moreover, Tie2-MFI was not significantly upregulated in any of the conditions compared with unstimulated control cells (**Fig. 4C** and **D**). These findings were confirmed at the mRNA level, which revealed no *Tie2* induction, nor robust expression of *Tie2* after culturing the cells for 24 hours under any of the conditions (**Fig. 4E** and **F**).

We reasoned that macrophage cell lines might be epigenetically restricted in their ability to express Tie2. We therefore isolated bone marrow-derived myeloid cells from Tie2-KO and Ctrl mice and cultured them *in vitro* under normoxia and hypoxic conditions. Similar to the macrophage cell lines, 24 hours of stimulation did not result in an upregulated Tie2 expression in bone marrow-derived myeloid cells (**Fig. 4G**).

As TEMs have been shown to induce Tie2 expression in various inflammatory settings (41, 42), we utilized an experimental model of acute zymosan-A induced peritonitis to further validate the findings made in culture cells. To this end, the inflammatory polysaccharide zymosan A was intraperitoneally injected into Tie2-KO and WT animals and the infiltrating immune cells were isolated 24 hours after treatment. Confirming the previous findings, no differences were

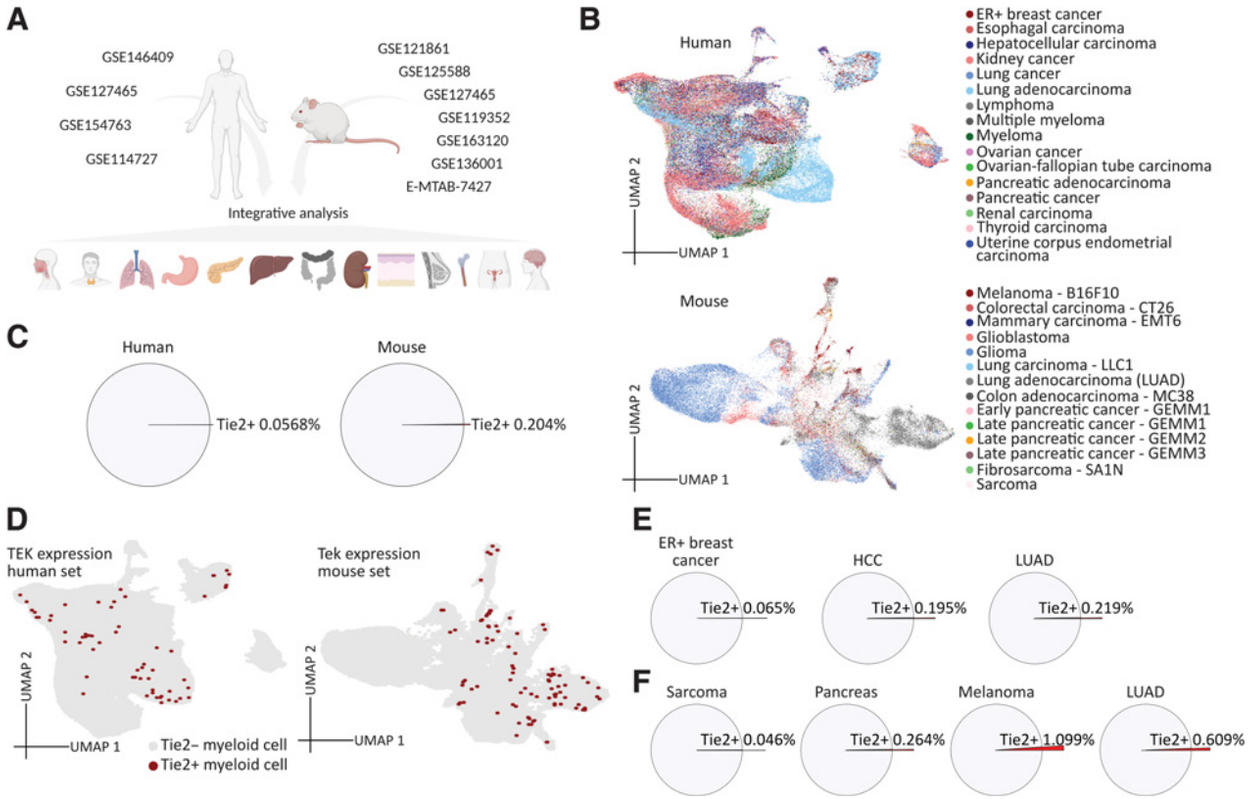

Figure 5.

A, Schematic overview of integration strategy and datasets and tumor entities included in the analysis. **B,** UMAP visualization of the integrated human (top) and mouse (bottom) dataset. Cells are colored according to tumor entity. **C,** Pie charts of Tie2-expressing myeloid cell frequencies in the total human (left) and total mouse (right) dataset. **D,** Visualization of the distribution of Tie2+ myeloid cells in the UMAP space of the total human (left) or total mouse (right) dataset. **E** and **F,** Pie charts of Tie2+ myeloid cell frequencies in cancer subsets that contain at least one cell with Tie2 expression within the human dataset (**E**) or the mouse dataset (**F**).

observed in the composition and absolute cell number of the myeloid immune infiltrate (Supplementary Fig. S3B). Furthermore, Tie2 expression was not detected on macrophages recruited to the inflammatory site by flow cytometry (Supplementary Fig. S3C).

Meta-analysis of mouse and human tumor scRNA-seq data provides no evidence for a Tie2-expressing subpopulation among TIMs

None of the experiments of this study had yielded any evidence for a functional contribution of macrophage-expressed Tie2 for tumor progression or therapy relapse and we even failed to induce macrophage Tie2 expression in supposedly solidly established induction protocols *in vitro* and *in vivo*. We consequently sought to confirm evidence for a functionally distinct TEMs population in an unbiased systematic meta-analysis approach of recently published scRNA-seq datasets of tumor-infiltrating myeloid cells. We integrated towards this end four human scRNA-seq datasets using a reciprocal principal component analysis (rPCA) approach, encompassing 16 distinct cancer entities and a total of 105,497 cells, as well as seven mouse datasets of 14 cancer entities and 45,519 cells (**Fig. 5A**). The myeloid identity of the cells was validated by congruent marker expression (*PTPRC*+, *ITGAM*+) and revealed the presence of macrophages (*LYZ*+, *CSF1R*+, *ADGRE1* high), monocytes (*LYZ*+, *CSF1R*+, *ADGRE1* low), and mast cells (*KIT* high; Supplementary Figs. S4A and S4B). Clustering analysis using a shared nearest-neighbor (SNN) algorithm with subsequent dimensional reduction by means of uniform manifold approximation and projection (UMAP) revealed transcriptional conservation of infiltrating myeloid cells, as cells from the distinct datasets were distributed rather homogenously in the two-dimensional space (**Fig. 5B**). Corresponding to our preclinical experiments, the frequency of Tie2-expressing myeloid cells was almost negligible for both the human dataset (60 cells in total, frequency of 0.06%) and the mouse dataset (94 cells in total, frequency of 0.2%; **Fig. 5C**).

As scRNA-seq is a low-resolution technology and data in general is sparse, we reasoned that if TEMs form a functionally distinct population and the expression of Tie2 may simply be below the detection limit, we would observe a cell cluster that is enriched for the few TEMs. To our surprise, this was not the case, as TEMs were distributed randomly in the UMAP and were not enriched in any specific subpopulation (**Fig. 5D**). This observation could not be attributed to the data integration algorithm, which at times masks biological observations by correcting for batch-effects, as subclustering of the unintegrated datasets containing more than one TEM did not reveal specifically enriched TEM clusters either (Supplementary Figs. S4C and S4D). Moreover, the majority of TEMs originated from one study characterizing myeloid infiltrates in lung adenocarcinoma (LUAD) in mice and humans (28). However, the frequency of TEMs was negligible for each of the individual datasets with a maximum of 0.22% of TEMs for human cancers and a maximum of 1.1% for mouse cancers (**Fig. 5E** and **F**). As TIMs are closely associated with vessels, we hypothesized that the detected Tie2 expression might be due to

cell–cell doublets that were not filtered out during the initial quality control. Recent scRNA-seq studies have identified Tie2 expression in multiple vessel-associated cell types (43, 44). We therefore established a marker gene panel for Tie2-expressing vessel cells comprising endothelial cell marker genes (*ERG*, *CLDN5*, *CDH5*, *PLVAP*, *NR2F2*, *HEY1*, *GJA4*, *GJA1*), mural cell marker genes (*PDGFRB*, *DES*, *COL4A2*, *MYH11*, *ACTA2*) and fibroblast marker genes (*PDGFRA*, *COL1A2*) and correlated the expression of the vascular gene set with the expression of *TEK* in the Tie2+ myeloid cell subset. For both the human and mouse dataset we found roughly one third of TEMs to be enriched for vascular genes. These TEMs showed positive correlation of *TEK* expression and the vascular gene set, pointing towards likely vascular cell-myeloid cell doublets (Supplementary Figs. S4E and S4F). Unexpectedly, vascular gene expressing TEMs did not cluster separately from vascular gene-negative TEMs, implicating that the vascular contribution to myeloid cell transcriptomes is either not sufficient to drive separation in the clustering algorithm, or that vascular gene-negative TEMs are vascular cell-myeloid cell doublets for which vascular genes are below the detection limit. Collectively, these data put the functional contribution of TEMs in question, as the frequency of TEMs among tumor-infiltrating myeloid cells was minimal and TEMs did not form a transcriptionally distinct subpopulation in our *in silico* analysis.

Discussion

The concept of an angiogenic bone marrow-derived macrophage population that expresses gene sets that were formerly described to be EC-specific is well established. Functionally, these macrophages infiltrate areas of hypoxia and acute inflammation along cytokine gradients and direct vascular repair and local angiogenesis through the secretion of VEGFA. Seminal work by Naldini and colleagues identified *Tie2* as a bona fide marker gene for this cell population (16, 45). In endothelial cells, the angiopoietin/Tie-signaling axis acts as a crucial mediator of vascular differentiation, maturation, and maintenance of the quiescent endothelial phenotype. Here, Ang1 serves as the agonistic ligand of Tie2 to promote vessel stability. In contrast, Ang2 acts as an antagonist of Ang1/Tie2 destabilizing endothelial cells and rendering them responsive to the activities of other vasculotropic cytokines such as VEGF. In macrophages, Ang2 does not appear to primarily signal via Tie2, because TEMs have been shown to migrate towards gradients of Ang2 and to acquire an activated state in an integrin-dependent manner (22, 24). Yet, macrophage-expressed Tie2 promotes cell survival through the phosphorylation of Akt. This survival benefit could be linked to the relapse mechanism in tumors after chemotherapy, as mice with genetic deletion of Tie2 in the myeloid lineage were not able to reconstruct the tumor vasculature in a model of fibrosarcoma after chemotherapy and failed to relapse (23). The experiments summarized in this study were set out to reproduce these findings. Yet, applying a plethora of different preclinical models, we failed to observe any differences in tumor relapse and re-vascularization between mice with Tie2 deficiency in myeloid cells and control animals. One important difference between the work by Chen and colleagues (23) and our study is the genetic strategy and the definition of control mice employed in both studies. Although we employed a mouse model with floxed sites for both *Tie2* alleles (*LysM-Cre*± × *Tie2floxed/floxed*), allowing for homozygosity of *Tie2* in all nonmyeloid cells, Chen and colleagues (23) used *LysM-Cre*+/+ × *Tie2-/floxed* as knockout animals and *LysM-Cre*+/+ × *Tie+/floxed* as controls. As such, control animals were homozygous for *Tie2* in the nonmyeloid lineage, whereas the knockout group was a global heterozygous knockout. The global homozygous knockout of *Tie2* leads to embryonic lethality at E10.5 (46) and although mice with Tie2 haploinsufficiency are viable and develop normally, $Tie2^{+/-}$ mice display vascular phenotypes during homeostasis (47, 48), which are aggravated under pathological conditions. These include a diminished vascular reperfusion after hind limb ischemia (49), a process previously shown to involve recruitment of TEMs (42), an attenuation of the endothelial inflammatory response after LPS treatment (50) and higher susceptibility of endothelial cells towards serotonin stimulation, resulting in increased cell death (47). The possibility that the observed phenotypes in Chen and colleagues (23) are driven by inherent vascular defects and an altered tumor vasculature in the knockout group, rather than the loss of myeloid cell-expressed *Tie2* is therefore highly likely. Either way, the comparison of heterozygous *Tie2* experimental mice with homozygous *Tie2* wild-type mice outside the myeloid lineage invalidates the experimental strategy employed by Chen and colleagues (23).

Functional expression of Tie2 in macrophages has also been reported in the context of tumor cell intravasation and metastatic dissemination (18, 19, 20). Here, TEMs form doorways consisting of a tumor cell, a blood or lymph EC and a TEM, creating an entry for tumor cells to the circulation by inducing localized transient vascular permeability via the secretion of VEGFA (18, 21). Systemic inhibition of Tie2 with rebastinib, a broad specificity kinase inhibitor with preference for Tie2, resolved such doorways and inhibited metastatic spread. In our well controlled genetic model of myeloid *Tie2* deletion, we could not identify significant changes in the metastatic burden of mice with myeloid cell specific *Tie2* deletion compared with controls, implying that the phenotypes driven by systemic treatment with rebastinib either stem from Tie2 inhibition in nonmyeloid cells, such as EC or perivascular cells, or through inhibition of any of the other drug targeted kinases. We have previously shown that deletion of pericyte-derived *Tie2* affects tumor angiogenesis and primary tumor growth (51). Similarly, deletion of *Tie2* in tumor lymphatics causes a disruption of the tumor lymphatic vascular system, which, in turn, blocks the lymphogenic route of metastasis (52), highlighting potential confounding factors of the systemic treatment approach using a small molecular weight tyrosine kinase inhibitor. It needs to be taken into account that all *in vivo* experiments in this study were performed with a constitutive Cre-line, which could have led to a developmental gene compensation of the *Tie2* deletion. This, however, seems rather unlikely, as the global or EC-specific homozygous and heterozygous knockout of *Tie2* are not compensated.

Moreover, throughout our study, we did not find evidence for robust Tie2 expression on macrophages. At the transcriptomic level, *Tie2* expression was below the detection limit for most samples, and samples with detectable amounts of *Tie2* mRNA displayed expression levels that were barely above the background signal. Although we consistently observed a small fraction of macrophages with high Tie2 expression in our FACS and IHC analyses, a similarly sized population could be found in knockout animals and in samples stained with a fluorescently labeled isotype control antibody. We therefore conclude that the Tie2+ macrophage population consists of either a highly autofluorescent subpopulation, or binds in an unspecific manner to the Fc-domain of the FACS antibody, a phenomenon that was previously reported for monocytes and macrophages and is not curbed by standard blockade of Fc-receptors prior to staining (53). This discrepancy of Tie2 staining and lack of mRNA expression was also observed in a recent study that specifically sorted tumor associated macrophages that had high Tie2 and low Tie2-staining intensity and performed bulk microarray analysis on the cellular subsets. Interestingly, while other proteins with high staining intensity were also

upregulated at the RNA level, *Tie2* was not found among the differentially regulated genes (54). Although protein and mRNA-expression may not always correlate, we recently identified close correlation of Tie2 protein and mRNA levels in the liver endothelium, where regulation of protein activity was exerted at the level of posttranslational modifications (55). The *in vitro* findings of this study further support the notion that macrophages lack the ability to express Tie2, because cultured macrophage cell lines and primary mouse bone marrow-derived macrophages failed to express Tie2 either following exposure to hypoxia or following stimulation with Ang2. These data are in contrast to earlier reports demonstrating activity of the *Tie2* promoter in bone marrow-derived TIMs (16). The Tie2 reporter construct employed in this study, however, was introduced into the genome by lentiviral gene transfer and not as a knock-in into the endogenous locus. Resolving these apparently contradicting findings, it may well be that macrophages may in principle be able to express *Tie2*, but the endogenous locus appears to be sealed under normal conditions. In a more plastic state, macrophages could then reacquire the ability to express *Tie2*, similar to more undifferentiated cells of the hematopoietic lineage.

To reconcile for the discrepancy of our study with earlier reports implying macrophage-expressed Tie2 in tumor progression, metastasis, and relapse from therapy, we employed an unbiased literature data-based meta-analytical approach to address, whether TIM express *Tie2*. We performed towards this end an *in silico* meta-analysis of scRNA-seq datasets obtained from human and mouse tumor-infiltrating myeloid cells. Similar to our targeted analyses, we were not able to identify a transcriptionally distinct macrophage subpopulation that was marked by robust *Tie2* expression in neither human nor mouse tumors. A limitation for any scRNA-seq analysis is the low sensitivity, which could cause false negative results. It can therefore not be excluded that macrophage-expressed Tie2 may simply be below the detection limit. This, however, seems unlikely, as recent scRNA-seq work identified and verified previously unappreciated *Tie2* expression on fibroblasts, skeletal muscle cells, vascular smooth muscle cells, and pericytes (43, 44, 56), validating the technology's suitability to detect *Tie2*-expressing cell types *de novo*. In addition, the few TEMs identified in the single-cell dataset were randomly distributed and not enriched in a specific subpopulation, rather pointing towards a sampling artefact. This was further supported by the finding that roughly one third of TIMs that expressed *Tie2* showed correlation with the expression of core identity genes of other Tie2-expressing cell types, indicating potential cell–cell doublets. Correspondingly, most TEMs were derived from one dataset sampling lung tumors, a tissue that requires harsh digestion conditions that can potentially induce endothelial cell death, which could cause RNA leakage and contamination in droplet based scRNA-seq approaches.

In conclusion, supported by (i) multiple independent tumor models employing a definite genetic strategy and involving primary tumor experiments, tumor-relapse following chemotherapy, and metastasis experiments involving primary tumor surgery; (ii) cellular experiments of Tie2 induction; and (iii) an extensive meta-analysis of published human and mouse tumor scRNA-seq data, this study unambiguously disproves the concept of macrophage-expressed Tie2 as a key regulator of tumor progression, metastasis and tumor relapse following chemotherapy. Instead, macrophages do not express functional Tie2 receptor and the previously proposed value of macrophage-expressed Tie2 as therapeutic target and prognostic marker deserves reconsideration.

Authors' Disclosures

H.G. Augustin reports grants from Deutsche Forschungsgemeinschaft (Collaborative Research Center CRC1366 "Vascular Control of Organ Function," project number 39404578), grants from Collaborative Research Center CRC1324 "Wnt signaling" (project number 331351713), and grants from European Research Council Advanced Grant "AngioMature" (project 787181) during the conduct of the study. No disclosures were reported by the other authors.

Authors' Contributions

M. Jakab: Conceptualization, data curation, formal analysis, validation, investigation, visualization, methodology, writing–original draft, writing–review and editing. **T. Rostalski:** Conceptualization, data curation, formal analysis, validation, investigation, visualization, methodology, writing–original draft, writing–review and editing. **K.H. Lee:** Data curation, validation, investigation, visualization, methodology, writing–review and editing. **C. Mogler:** Conceptualization, data curation, formal analysis, validation, investigation, methodology. **H.G. Augustin:** Conceptualization, resources, data curation, supervision, funding acquisition, validation, visualization, writing–original draft, writing–review and editing.

Acknowledgments

The authors thank Celine Rausch and Clara Mai for their excellent technical assistance. The DKFZ flow cytometry, light microscopy, and laboratory animal core facilities are gratefully acknowledged for their excellent support. The schematic overview in **Fig. 5A** was created with BioRender.com.

The costs of publication of this article were defrayed in part by the payment of page charges. This article must therefore be hereby marked *advertisement* in accordance with 18 U.S.C. Section 1734 solely to indicate this fact.

Received September 22, 2021; revised December 5, 2021; accepted January 18, 2022; published first April 4, 2022.

References

1. Miller KD, Nogueira L, Mariotto AB, Rowland JH, Yabroff KR, Alfano CM, et al. Cancer treatment and survivorship statistics, 2019. CA Cancer J Clin 2019;69:363–85.
2. D'Alterio C, Scala S, Sozzi G, Roz L, Bertolini G. Paradoxical effects of chemotherapy on tumor relapse and metastasis promotion. Sem Cancer Biol 2020;60:351–61.
3. Semenza GL. Targeting HIF-1 for cancer therapy. Nat Rev Cancer 2003;3:721–32.
4. Kerbel RS. Tumor angiogenesis. New Engl J Med 2008;358:2039–49.
5. Ahn GO, Brown JM. Role of endothelial progenitors and other bone marrow-derived cells in the development of the tumor vasculature. Angiogenesis 2009;12:159–64.
6. Asahara T, Murohara T, Sullivan A, Silver M, van der Zee R, Li T, et al. Isolation of putative progenitor endothelial cells for angiogenesis. Science 1997;275:964–7.
7. Rafii S, Lyden D. Therapeutic stem and progenitor cell transplantation for organ vascularization and regeneration. Nat Med 2003;9:702–12.
8. George AL, Bangalore-Prakash P, Rajoria S, Suriano R, Shanmugam A, Mittelman A, et al. Endothelial progenitor cell biology in disease and tissue regeneration. J Hemat Oncol 2011;4:24.
9. Purhonen S, Palm J, Rossi D, Kaskenpää N, Rajantie I, Ylä-Herttuala S, et al. Bone marrow-derived circulating endothelial precursors do not contribute to vascular endothelium and are not needed for tumor growth. Proc Natl Acad Sci U S A 2008;105:6620–5.
10. Kerbel RS, Benezra R, Lyden DC, Hattori K, Heissig B, Nolan DJ, et al. Endothelial progenitor cells are cellular hubs essential for neoangiogenesis of certain aggressive adenocarcinomas and metastatic transition but not adenomas. Proc Natl Acad Sci U S A 2008;105:E54;Author reply E5.
11. Horrevoets AJ. Angiogenic monocytes: another colorful blow to endothelial progenitors. Am J Pathol 2009;174:1594–6.
12. Urbich C, Heeschen C, Aicher A, Dernbach E, Zeiher AM, Dimmeler S. Relevance of monocytic features for neovascularization capacity of circulating endothelial progenitor cells. Circulation 2003;108:2511–6.

13. Kim SJ, Kim JS, Papadopoulos J, Wook Kim S, Maya M, Zhang F, et al. Circulating monocytes expressing CD31: implications for acute and chronic angiogenesis. Am J Pathol 2009;174:1972–80.
14. Kioi M, Vogel H, Schultz G, Hoffman RM, Harsh GR, Brown JM. Inhibition of vasculogenesis, but not angiogenesis, prevents the recurrence of glioblastoma after irradiation in mice. J Clin Invest 2010;120:694–705.
15. Schmeisser A, Garlichs CD, Zhang H, Eskafi S, Graffy C, Ludwig J, et al. Monocytes coexpress endothelial and macrophagocytic lineage markers and form cord-like structures in Matrigel under angiogenic conditions. Cardiovasc Res 2001;49:671–80.
16. De Palma M, Venneri MA, Galli R, Sergi Sergi L, Politi LS, Sampaolesi M, et al. Tie2 identifies a hematopoietic lineage of proangiogenic monocytes required for tumor vessel formation and a mesenchymal population of pericyte progenitors. Cancer Cell 2005;8:211–26.
17. De Palma M, Mazzieri R, Politi LS, Pucci F, Zonari E, Sitia G, et al. Tumor-targeted interferon-alpha delivery by Tie2-expressing monocytes inhibits tumor growth and metastasis. Cancer Cell 2008;14:299–311.
18. Harney AS, Arwert EN, Entenberg D, Wang Y, Guo P, Qian BZ, et al. Real-time imaging reveals local, transient vascular permeability, and tumor cell intravasation stimulated by TIE2hi macrophage-derived VEGFA. Cancer Discov 2015;5:932–43.
19. Karagiannis GS, Pastoriza JM, Wang Y, Harney AS, Entenberg D, Pignatelli J, et al. Neoadjuvant chemotherapy induces breast cancer metastasis through a TMEM-mediated mechanism. Sci Transl Med 2017;9:eaan0026.
20. Harney AS, Karagiannis GS, Pignatelli J, Smith BD, Kadioglu E, Wise SC, et al. The selective Tie2 inhibitor Rebastinib blocks recruitment and function of Tie2(Hi) macrophages in breast cancer and pancreatic neuroendocrine tumors. Mol Cancer Ther 2017;16:2486–501.
21. Coste A, Karagiannis GS, Wang Y, Xue EA, Lin Y, Skobe M, et al. Hematogenous dissemination of breast cancer cells from lymph nodes is mediated by tumor microenvironment of metastasis doorways. Front Oncol 2020;10:571100.
22. Scholz A, Lang V, Henschler R, Czabanka M, Vajkoczy P, Chavakis E, et al. Angiopoietin-2 promotes myeloid cell infiltration in a β-integrin-dependent manner. Blood 2011;118:5050–9.
23. Chen L, Li J, Wang F, Dai C, Wu F, Liu X, et al. Tie2 expression on macrophages is required for blood vessel reconstruction and tumor relapse after chemotherapy. Cancer Res 2016;76:6828–38.
24. Srivastava K, Hu J, Korn C, Savant S, Teichert M, Kapel SS, et al. Postsurgical adjuvant tumor therapy by combining anti-angiopoietin-2 and metronomic chemotherapy limits metastatic growth. Cancer Cell 2014;26:880–95.
25. Goede V, Coutelle O, Shimabukuro-Vornhagen A, Holtick U, Neuneier J, Koslowsky TC, et al. Analysis of Tie2-expressing monocytes (TEM) in patients with colorectal cancer. Cancer Invest 2012;30:225–30.
26. Savant S, La Porta S, Budnik A, Busch K, Hu J, Tisch N, et al. The orphan receptor tie1 controls angiogenesis and vascular remodeling by differentially regulating Tie2 in tip and stalk cells. Cell Rep 2015;12:1761–73.
27. Massalha H, Bahar Halpern K, Abu-Gazala S, Jana T, Massasa EE, Moor AE, et al. A single cell atlas of the human liver tumor microenvironment. Mol Syst Biol 2020;16:e9682.
28. Zilionis R, Engblom C, Pfirschke C, Savova V, Zemmour D, Saatcioglu HD, et al. Single-cell transcriptomics of human and mouse lung cancers reveals conserved myeloid populations across individuals and species. Immunity 2019;50:1317–34.
29. Cheng S, Li Z, Gao R, Xing B, Gao Y, Yang Y, et al. A pan-cancer single-cell transcriptional atlas of tumor-infiltrating myeloid cells. Cell 2021;184:792–809.
30. Azizi E, Carr AJ, Plitas G, Cornish AE, Konopacki C, Prabhakaran S, et al. Single-cell map of diverse immune phenotypes in the breast tumor microenvironment. Cell 2018;174:1293–308.
31. Kumar MP, Du J, Lagoudas G, Jiao Y, Sawyer A, Drummond DC, et al. Analysis of single-cell RNA-Seq identifies cell-cell communication associated with tumor characteristics. Cell Rep 2018;25:1458–68.
32. Hosein AN, Huang H, Wang Z, Parmar K, Du W, Huang J, et al. Cellular heterogeneity during mouse pancreatic ductal adenocarcinoma progression at single-cell resolution. JCI Insight 2019;5:e129212.
33. Gubin MM, Esaulova E, Ward JP, Malkova ON, Runci D, Wong P, et al. High-dimensional analysis delineates myeloid and lymphoid compartment remodeling during successful immune-checkpoint cancer therapy. Cell 2018;175:1014–30.
34. Pombo Antunes AR, Scheyltjens I, Lodi F, Messiaen J, Antoranz A, Duerinck J, et al. Single-cell profiling of myeloid cells in glioblastoma across species and disease stage reveals macrophage competition and specialization. Nat Neurosci 2021;24:595–610.
35. Ochocka N, Segit P, Walentynowicz KA, Wojnicki K, Cyranowski S, Swatler J, et al. Single-cell RNA sequencing reveals functional heterogeneity of glioma-associated brain macrophages. Nat Commun 2021;12:1151.
36. Davidson S, Efremova M, Riedel A, Mahata B, Pramanik J, Huuhtanen J, et al. Single-cell RNA sequencing reveals a dynamic stromal niche that supports tumor growth. Cell Rep 2020;31:107628.
37. Hao Y, Hao S, Andersen-Nissen E, Mauck WM 3rd, Zheng S, Butler A, et al. Integrated analysis of multimodal single-cell data. Cell 2021;184:3573–87.
38. McCubbrey AL, Allison KC, Lee-Sherick AB, Jakubzick CV, Janssen WJ. Promoter specificity and efficacy in conditional and inducible transgenic targeting of lung macrophages. Front Immunol 2017;8:1618.
39. Mazzieri R, Pucci F, Moi D, Zonari E, Ranghetti A, Berti A, et al. Targeting the ANG2/TIE2 axis inhibits tumor growth and metastasis by impairing angiogenesis and disabling rebounds of proangiogenic myeloid cells. Cancer Cell 2011;19:512–26.
40. Hughes R, Qian B-Z, Rowan C, Muthana M, Keklikoglou I, Olson OC, et al. Perivascular M2 macrophages stimulate tumor relapse after chemotherapy. Cancer Res 2015;75:3479–91.
41. Ehrentraut H, Weisheit C, Scheck M, Frede S, Hilbert T. Experimental murine acute lung injury induces increase of pulmonary TIE2-expressing macrophages. J Inflam 2018;15:12.
42. Patel AS, Smith A, Nucera S, Biziato D, Saha P, Attia RQ, et al. TIE2-expressing monocytes/macrophages regulate revascularization of the ischemic limb. EMBO Mol Med 2013;5:858–69.
43. Vanlandewijck M, He L, Mäe MA, Andrae J, Ando K, Del Gaudio F, et al. A molecular atlas of cell types and zonation in the brain vasculature. Nature 2018;554:475–80.
44. Muhl L, Genové G, Leptidis S, Liu J, He L, Mocci G, et al. Single-cell analysis uncovers fibroblast heterogeneity and criteria for fibroblast and mural cell identification and discrimination. Nat Commun 2020;11:3953.
45. Venneri MA, De Palma M, Ponzoni M, Pucci F, Scielzo C, Zonari E, et al. Identification of proangiogenic TIE2-expressing monocytes (TEMs) in human peripheral blood and cancer. Blood 2007;109:5276–85.
46. Sato TN, Tozawa Y, Deutsch U, Wolburg-Buchholz K, Fujiwara Y, Gendron-Maguire M, et al. Distinct roles of the receptor tyrosine kinases Tie-1 and Tie-2 in blood vessel formation. Nature 1995;376:70–4.
47. Kugathasan L, Ray JB, Deng Y, Rezaei E, Dumont DJ, Stewart DJ. The angiopietin-1-Tie2 pathway prevents rather than promotes pulmonary arterial hypertension in transgenic mice. J Exp Med 2009;206:2221–34.
48. Thomson BR, Carota IA, Souma T, Soman S, Vestweber D, Quaggin SE. Targeting the vascular-specific phosphatase PTPRB protects against retinal ganglion cell loss in a pre-clinical model of glaucoma. Elife 2019;8:e48474.
49. Lekas M, Lekas P, Mei SH, Deng Y, Dumont DJ, Stewart DJ. Tie2-dependent neovascularization of the ischemic hindlimb is mediated by angiopoietin-2. PLoS One 2012;7:e43568.
50. Jongman RM, Zwiers PJ, van de Sluis B, van der Laan M, Moser J, Zijlstra JG, et al. Partial deletion of Tie2 affects microvascular endothelial responses to critical illness in a vascular bed and organ-specific way. Shock 2019;51:757–69.
51. Teichert M, Milde L, Holm A, Stanicek L, Gengenbacher N, Savant S, et al. Pericyte-expressed Tie2 controls angiogenesis and vessel maturation. Nat Commun 2017;8:16106.
52. Gengenbacher N, Singhal M, Mogler C, Hai L, Milde L, Pari AAA, et al. Timed Ang2-targeted therapy identifies the Angiopoietin-Tie pathway as key regulator of fatal lymphogenous metastasis. Cancer Discov 2021;11:424–45.
53. Andersen MN, SN A-K, Kragstrup TW, Hokland M. Elimination of erroneous results in flow cytometry caused by antibody binding to Fc receptors on human monocytes and macrophages. Cytometry Part A 2016;89:1001–9.
54. Consonni FM, Bleve A, Totaro MG, Storto M, Kunderfranco P, Termanini A, et al. Heme catabolism by tumor-associated macrophages controls metastasis formation. Nat Immunol 2021;22:595–606.
55. Inverso D, Shi J, Lee KH, Jakab M, Ben-Moshe S, Kulkarni SR, et al. A spatial vascular transcriptomic, proteomic, and phosphoproteomic atlas unveils an angiocrine Tie-Wnt signaling axis in the liver. Dev Cell 2021;56:1677–93.
56. Kalluri AS, Vellarikkal SK, Edelman ER, Nguyen L, Subramanian A, Ellinor PT, et al. Single-cell analysis of the normal mouse aorta reveals functionally distinct endothelial cell populations. Circulation 2019;140:147–63.